2026 • Vol. 4, No. 1 • pp. 10-15
Future Dental Research (FDR)

Print ISSN: 3006-0516
Online ISSN: 3006-0354
NABEA AL-AJYAL FOUNDATION PRESS
Future Dental Research (FDR)

Comparative In Vitro Evaluation of Hydroxyapatite, β-Tricalcium Phosphate, Biphasic Calcium Phosphate, and Strontium-Doped Hydroxyapatite as Bioceramic Bone Substitutes for Dental and Maxillofacial Bone Regeneration

Sarah Al-Rihaymee*

Department of Periodontics, College of Dentistry, University of Babylon, Hillah 51002, Iraq
**Corresponding Email:* sarra.anwar1205a@codental.uobaghdad.edu.iq

Access this article online

ORIGINAL A R T I C L E
Received: 20.04.2026 **Revised:** 20.05.2026
Accepted: 10.06.2026
DOI: 10.57238/fdr.2026.152576.1002

OPEN ACCESS

ABSTRACT

Background: Bioceramic bone substitutes are central to contemporary dental bone regeneration, but the relative physicochemical, mechanical, and biological merits of stoichiometric hydroxyapatite (HA), β-tricalcium phosphate (β-TCP), biphasic calcium phosphate (BCP), and strontium-doped HA (Sr-HA) remain insufficiently characterized within a single, controlled in vitro framework. This study compared four laboratory-synthesized bioceramic granules under identical processing and testing conditions. Methods: HA, β-TCP, BCP (60/40 HA: β-TCP), and 5 mol% Sr-HA powders were synthesized by aqueous chemical precipitation, calcined at 900 °C, and sintered as 5 × 5 × 5 mm granules at 1150 °C. Phase composition was determined by XRD; functional groups by FTIR; morphology and elemental ratios by SEM-EDS; surface area by BET. Mechanical strength and porosity were quantified; in vitro bioactivity was assessed by 14-day SBF immersion; degradation by 28-day Tris-HCl weight loss. MG-63 cell viability (MTT, ISO 10993-5), ALP activity, and Alizarin Red S mineralization were evaluated. Antibacterial activity was tested against S. aureus ATCC 25923 and E. coli ATCC 25922 by agar diffusion. Data (n = 6) were analyzed by one-way ANOVA and Tukey's test (α = 0.05). Results: XRD confirmed phase-pure compositions. Compressive strength differed significantly ($p < 0.001$): HA 8.7 ± 0.6 MPa > BCP 6.4 ± 0.5 > Sr-HA 5.9 ± 0.5 > β-TCP 3.1 ± 0.4 MPa. Twenty-eight-day weight loss was highest for β-TCP (18.4 ± 1.6%) and lowest for HA (4.2 ± 0.5%). All materials were non-cytotoxic (≥88% viability). Sr-HA produced the highest MG-63 proliferation at 168 h (138.7 ± 7.4%; $p < 0.05$), ALP activity (1.54-fold over HA at Day 14; $p < 0.001$), mineralization ($p < 0.001$), and the only measurable antibacterial inhibition (S. aureus 4.3 ± 0.6 mm; E. coli 3.7 ± 0.5 mm). Conclusion: No single material was optimal across all dimensions. Sr-HA provided the most favorable biological profile; BCP offered the best mechanical-resorption balance. A defect-matched clinical decision framework is proposed.

Keywords: Bioceramics, Biphasic Calcium Phosphate, Dental Bone Regeneration, hydroxyapatite, in Vitro Bioactivity, MG-63 Osteoblasts, Strontium-Doped Hydroxyapatite

1 Introduction

THE reconstruction of alveolar and craniomaxillofacial bone defects following tooth extraction, periodontal disease, peri-implantitis, or trauma is one of the most frequent regenerative challenges in modern dentistry. Following tooth extraction, the buccal alveolar plate undergoes pronounced resorption; systematic reviews report horizontal bone loss of 29–63% and vertical loss of 11–22% within 6 months [1]. Such dimensional changes frequently compromise implant placement, driving adoption of

alveolar ridge preservation (ARP) and guided bone regeneration (GBR) [2]. The global dental bone graft substitutes market is valued at approximately USD 1.40 billion in 2026 and projected to reach USD 2.04 billion by 2031 [3], with bioceramics accounting for a rising share.

Autogenous bone remains the gold standard—it is simultaneously osteogenic, osteoinductive, and osteoconductive—but donor-site morbidity, limited intraoral harvest volume, and increased operative time have driven development of synthetic alternatives [4, 5]. Hydroxyapatite [$Ca_{10}(PO_4)_6(OH)_2$, HA], with a Ca/P molar ratio of 1.67, provides stable osteoconductive scaffolds [6], but its low solubility translates into very slow in vivo resorption [7]. β-Tricalcium phosphate [β-$Ca_3(PO_4)_2$, β-TCP] has a Ca/P ratio of 1.50 and is approximately ten times more soluble; it is resorbed and replaced by vital bone within 6–12 months in favourable defects [8]. Biphasic calcium phosphate (BCP) mixtures combine the complementary properties of both phases; the 60/40 HA/β-TCP ratio underlies several widely used commercial grafts [9].

Strontium (Sr^{2+}) substituion in HA simultaneously stimulates osteoblastic bone formation and inhibits osteoclastic resorption—the mechanistic basis for strontium ranelate [10, 11]. Incorporated at 1–10 mol%, strontium increases osteoblast proliferation and differentiation marker expression [12, 13]. Additional substituents include zinc (antibacterial/osteogenic), silicon (osteostimulatory), and magnesium (improves sintering) [14, 15, 16, 17]. Despite the volume of literature on individual bioceramics, directly matched, multi-parameter in vitro comparisons under standardized processing remain scarce. The aim of this study was to compare HA, β-TCP, BCP (60/40), and 5 mol% Sr-HA prepared identically across physicochemical, mechanical, and biological dimensions. The null hypothesis was that no differences exist between groups in any measured parameter.

2 Materials and Methods

2.1 Reagents and study design

All chemicals (calcium nitrate tetrahydrate, diammonium hydrogen phosphate, strontium nitrate, ammonium hydroxide, Tris, analytical-grade SBF salts) were from Sigma-Aldrich (St. Louis, MO, USA). Ultrapure deionized water (18.2 MΩ·cm, Milli-Q, Merck) was used throughout. The study was a fully randomized in vitro design: four groups (HA, β-TCP, BCP 60:40, 5 mol% Sr-HA), n = 6 specimens per group per assay.

2.2 Synthesis of Bioceramic Powders

HA was prepared by aqueous precipitation at Ca/P = 1.67, pH 10.5, 60 °C, aged 24 h, dried 105 °C, calcined 900 °C/2 h. β-TCP: Ca/P = 1.50, pH 7.5, calcination hold at 1100 °C. BCP: planetary ball-milling HA and β-TCP 60:40 (200 rpm, 2 h, zirconia jars). Sr-HA: as HA with 5 mol% Ca replaced by $Sr(NO_3)_2$ at (Ca + Sr)/P = 1.67.

2.3 Granule Fabrication and Sintering

Powders uniaxially pressed (200 MPa) into 5 × 5 × 5 mm green bodies with 2 wt% PVA binder and 10 wt% camphor porogen. Debinded 600 °C (1 h); sintered 1150 °C (3 h) in air at 3 °C/min.

2.4 Physicochemical Characterization

XRD: Rigaku Ultima IV (Cu Kα, 2θ = 10–60°); JCPDS 09-0432 (HA), 09-0169 (β-TCP). FTIR: PerkinElmer Spectrum Two (4000–400 cm^{-1}, KBr pellet). SEM-EDS: Hitachi SU-3500 at 15 kV. BET: Micromeritics ASAP 2020. Apparent porosity: Archimedes method (n = 6).

2.5 Mechanical Testing

Uniaxial compressive strength: Shimadzu AGS-X (1 kN, 0.5 mm/min), six 5 × 5 × 5 mm specimens per group.

2.6 In Vitro Bioactivity in SBF

Kokubo-Takadama SBF (pH 7.40, 36.5 °C) [18, 19]. Granules immersed at 0.1 cm^{-1} surface-area-to-volume ratio, refreshed every 48 h; retrieved at days 1, 7, 14 for SEM and FTIR.

2.7 In Vitro Degradation

Pre-weighed granules immersed in 0.05 M Tris-HCl (pH 7.40, 37 °C); retrieved at 7, 14, 21, 28 days. WL% = $(W_0 - W_t)/W_0 \times 100$ after drying at 60 °C.

2.8 Cell Culture and Biological Evaluation

MG-63 cells (ATCC CRL-1427) in DMEM/10% FBS/1% pen-strep at 37 °C/5% CO_2, passages 4–8. Granules autoclaved 121 °C/20 min, pre-incubated 24 h. MTT cytotoxicity per ISO 10993-5: 0.2 g/mL extract, 24–168 h exposure, viability ≥ 70% = non-cytotoxic. ALP activity (p-nitrophenyl phosphate substrate) after 7 and 14 days of osteogenic culture, normalized to total protein (BCA). Alizarin Red S staining after 21 days; cell-free apatite background subtracted.

2.9 Antibacterial Activity

Agar well diffusion vs S. aureus ATCC 25923 and E. coli ATCC 25922 (0.5 McFarland). Sterilized granules (100 mg) in 6 mm wells; 37 °C/24 h; inhibition zone diameter recorded.

2.10 Statistical Analysis

Mean ± SD (n = 6). Normality: Shapiro-Wilk; homoscedasticity: Levene's test. One-way ANOVA + Tukey's HSD; two-way ANOVA for time-course. SPSS v.26; α = 0.05.

3 Results

3.1 Phase Composition and Crystallinity (XRD)

XRD confirmed single-phase HA ($P6_3/m$, JCPDS 09-0432), phase-pure β-TCP (R3c, JCPDS 09-0169), and Rietveld-validated 61.4 ± 1.8 wt% HA / 38.6 ± 1.8 wt% β-TCP for BCP. Sr-HA showed HA-like patterns with a reproducible (211) reflection shift of $\Delta 2\theta \approx -0.12°$, consistent with lattice expansion from Ca^{2+} (r = 1.00 Å) substitution by the larger Sr^{2+} (r = 1.18 Å). Crystallite size (Scherrer): HA 48.6 ± 3.2 nm; β-TCP 67.4 ± 4.1 nm; BCP 51.8 ± 3.8 nm; Sr-HA 39.2 ± 2.9 nm ($p < 0.05$). Full data are in Table 1.

Table 1. Physicochemical and mechanical properties of the four bioceramic granules (mean ± SD, n = 6).

Property	HA	β-TCP	BCP (60/40)	Sr-HA (5 mol%)
Ca/P molar ratio (EDS)	1.66 ± 0.03	1.50 ± 0.02	1.61 ± 0.03	1.67 ± 0.03 (Ca + Sr)/P
Crystallite size (nm)	48.6 ± 3.2	67.4 ± 4.1	51.8 ± 3.8	39.2 ± 2.9 ✓ smallest
BET surface area (m^2/g)	4.8 ± 0.4	6.2 ± 0.5	5.4 ± 0.4	7.9 ± 0.6 ✓ highest
Total porosity (%)	67.8 ± 2.1	71.8 ± 1.9	69.4 ± 1.7	66.4 ± 2.3
Bulk density (g/cm^3)	1.01 ± 0.04	0.87 ± 0.05	0.95 ± 0.04	1.06 ± 0.04
Compressive strength (MPa)	8.7 ± 0.6 ★ highest	3.1 ± 0.4 ▼ lowest	6.4 ± 0.5	5.9 ± 0.5
28-day weight loss (%)	4.2 ± 0.5 ● slowest	18.4 ± 1.6 ▲ fastest	11.7 ± 1.1	6.8 ± 0.7
Macropore size (µm)	190–400	200–420	185–410	180–390
Mean grain size (µm)	1.8 ± 0.4	3.2 ± 0.7	2.1 ± 0.5	1.3 ± 0.3 ✓ finest

★ = significantly highest; ▼ = significantly lowest; ✓ = significantly different from HA (Tukey, $p < 0.05$).

3.2 FTIR Spectroscopy

HA, BCP, and Sr-HA showed apatite phosphate bands (ν_3 1090/1030 cm^{-1}; ν_1 962 cm^{-1}; ν_4 601/565 cm^{-1}) and OH^- stretching/libration at 3572/632 cm^{-1}. Sr-HA showed reduced OH^- intensity consistent with Sr^{2+}-induced lattice distortion. β-TCP exhibited split phosphate bands (1120, 1042, 945 cm^{-1}) without OH^- libration.

3.3 Morphology, Elemental Composition, and Surface Area

SEM revealed interconnected macroporous architectures (mean 263 ± 48 µm, range 180–420 µm). HA grains rounded (1.8 ± 0.4 µm); β-TCP larger/angular (3.2 ± 0.7 µm); Sr-HA finest grains (1.3 ± 0.3 µm) with roughest surface. EDS confirmed Ca/P ratios matching nominal compositions. BET surface areas: 4.8 → 7.9 m^2/g (Sr-HA, significantly highest; $p < 0.001$).

3.4 Porosity and Mechanical Properties

Total porosity similar across groups (66.4–71.8%, $p = 0.07$). Compressive strength (ANOVA $F = 71.2$, $p < 0.001$): HA 8.7 ± 0.6 MPa > BCP 6.4 ± 0.5 > Sr-HA 5.9 ± 0.5 > β-TCP 3.1 ± 0.4 MPa. All values lie within the human trabecular bone range (2–12 MPa).

3.5 In Vitro Bioactivity (SBF)

Day 7: cauliflower apatite globules on Sr-HA and β-TCP; partial BCP coverage; sparse HA nucleation. Day 14: complete apatite coverage on β-TCP, Sr-HA, BCP; ~60% on HA. FTIR confirmed carbonated apatite. Bioactivity ranking: β-TCP ≈ Sr-HA > BCP > HA.

3.6 Degradation (Tris-HCl)

Cumulative 28-day weight loss: β-TCP 18.4 ± 1.6% > BCP 11.7 ± 1.1% > Sr-HA 6.8 ± 0.7% > HA 4.2 ± 0.5% (all pairwise $p < 0.01$). β-TCP showed an initial fast phase (0–7 days) then slower kinetics; HA and Sr-HA were approximately linear (Figure 1).

3.7 Cytocompatibility (MTT)

All materials produced ≥ 88% MG-63 viability at all time points (ISO 10993-5 threshold: ≥ 70%). At 168 h, Sr-HA produced 138.7 ± 7.4% of control—significantly higher than all groups from 72 h onward ($p < 0.05$); BCP significantly higher than HA and β-TCP at 168 h ($p < 0.05$). Data in Table 2.

3.8 ALP activity and mineralization

Sr-HA: 1.42-fold ALP over HA at Day 7 ($p < 0.01$); 1.54-fold at Day 14 ($p < 0.001$). BCP significantly higher than HA at both time points ($p < 0.05$). Alizarin Red S OD: Sr-HA (0.74 ± 0.07) > BCP (0.56 ± 0.06) > β-TCP (0.41 ± 0.05) > HA (0.32 ± 0.04); Sr-HA vs all others $p < 0.001$ (Figure 2).

3.9 Antibacterial Activity

Only Sr-HA produced measurable inhibition zones (S. aureus 4.3 ± 0.6 mm; E. coli 3.7 ± 0.5 mm; $p < 0.001$ vs all other groups). HA, β-TCP, and BCP: no inhibition (0.0 mm) (Table 3).

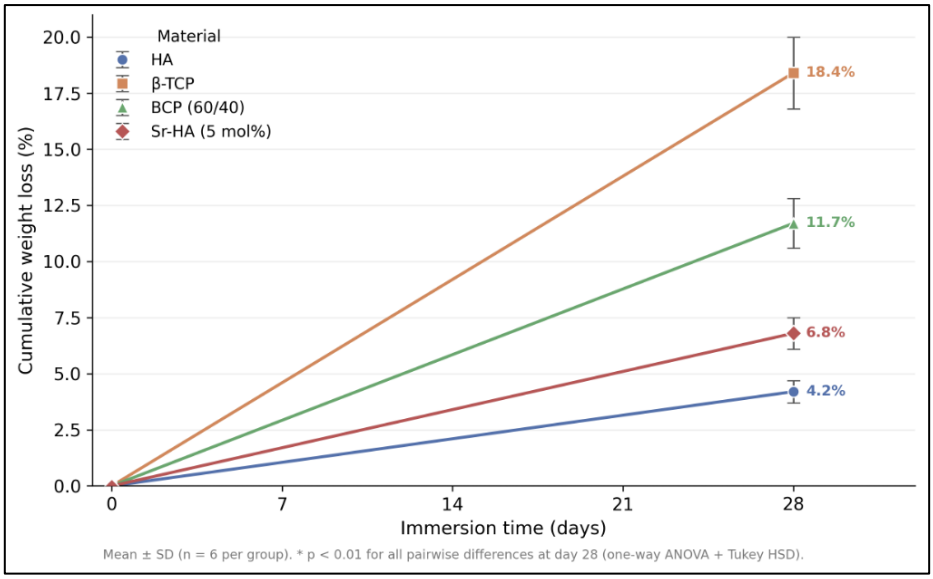

Fig. 1.

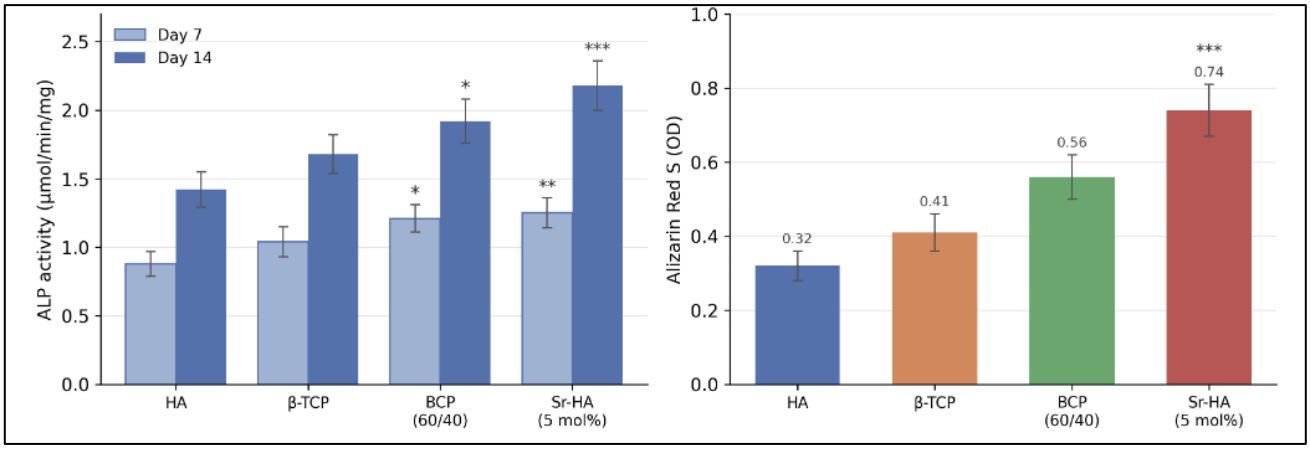

(a) (b)

Fig. 2. (a) ALP activity, (b) Mineralization – Alizarin red S (day 21).

Table 2. MG-63 cell viability (MTT), ALP activity, and Alizarin Red S (ARS) mineralization for the four bioceramic groups (n = 6).

Parameter / Time	HA	β-TCP	BCP	Sr-HA
Cell viability 24 h (%)	91.4 ± 4.6	89.2 ± 5.1	94.6 ± 4.2	102.8 ± 5.4
Cell viability 72 h (%)	97.2 ± 5.3	95.8 ± 4.9	110.4 ± 6.1	121.3 ± 6.6
Cell viability 168 h (%)	108.4 ± 6.8	101.6 ± 6.2	119.7 ± 7.1	138.7 ± 7.4 ★
ALP activity Day 7 (µmol/min/mg)	0.88 ± 0.09	1.04 ± 0.11	1.21 ± 0.10	1.25 ± 0.11 ★
ALP activity Day 14 (µmol/min/mg)	1.42 ± 0.13	1.68 ± 0.14	1.92 ± 0.16	2.18 ± 0.18 ★
Alizarin Red S OD Day 21	0.32 ± 0.04	0.41 ± 0.05	0.56 ± 0.06	0.74 ± 0.07 ★

★ = significantly highest value in each row (Tukey, $p < 0.05$).

Table 3. Agar well diffusion inhibition zones (mm) against S. aureus ATCC 25923 and E. coli ATCC 25922 (n = 6).

Material	S. aureus zone (mm)	E. coli zone (mm)	Interpretation
HA	0.0 ± 0.0	0.0 ± 0.0	No inhibition
β-TCP	0.0 ± 0.0	0.0 ± 0.0	No inhibition
BCP (60/40)	0.0 ± 0.0	0.0 ± 0.0	No inhibition
Sr-HA (5 mol%)	4.3 ± 0.6 *	3.7 ± 0.5 *	Mild inhibition ✓

* $p < 0.001$ vs HA, β-TCP, and BCP (one-way ANOVA + Tukey).

4 Discussion

4.1 Phase Composition and Microstructure

XRD confirmed that wet chemical precipitation followed by sintering at 1150 °C reliably produced phase-pure bioceramics [20]. The (211) lattice expansion in Sr-HA ($\Delta 2\theta \approx -0.12°$) replicates the magnitude reported by Frasnelli et al. [21] and confirms successful substitution rather than

surface adsorption. Reduced OH^- band intensity mirrors Capuccini et al. [22], who attributed it to the larger Sr^{2+} radius disrupting the hydroxyl channel. The smallest crystallite size in Sr-HA (39.2 nm vs 48.6 nm for HA) reflects the documented crystal-growth-inhibiting effect of strontium [11, 22]. Comparable total porosity across groups (66.4–71.8%) ensured mechanical and biological differences were attributable to material chemistry rather than scaffold architecture—a critical control rarely achieved comparing commercial products made by different proprietary routes.

4.2 Mechanical Strength vs. Resorption Rate

HA compressive strength (8.7 MPa at ~68% porosity) and the substantially lower β-TCP value (3.1 MPa) reproduce the documented inverse relationship between Ca/P ratio and mechanical weakness [23, 24]. β-TCP's rapid 28-day degradation (18.4%) is consistent with Diez-Escudero et al. [25], who showed that Ca/P ratio, crystallinity, and specific surface area jointly govern in vitro resorbability. The intermediate BCP behavior confirms that HA/β-TCP mixing provides tunability—the 60/40 ratio underpins the dominant clinical position of BCP, supported by Lee et al.'s 2025 network meta-analysis [9] showing comparable histomorphometric bone formation to autografts and xenografts [26]. All values fall within the human trabecular bone range (2–12 MPa), confirming suitability for non-load-bearing applications.

4.3 Biological Performance: The Case for Ion Substitution

All four materials satisfied ISO 10993-5 non-cytotoxicity criteria (viability ≥ 70%). Sr-HA produced markedly superior MG-63 proliferation, ALP, and mineralization, consistent with the dual osteoanabolic mechanism of Sr^{2+}: CaSR activation on osteoblasts stimulates Runx2, ALP, OCN, and COL-I expression, while OPG upregulation and RANKL inhibition suppress osteoclastogenesis [10, 27]. The 1.42-fold ALP increase at Day 7 closely matches the ~1.4-fold reported by Tsai et al. [12] for 5%-Sr-HA nanofibrous matrices. BCP's superiority over HA and β-TCP in differentiation reflects synergistic Ca^{2+}/PO_4^{3-} release from the β-TCP phase driving osteoblast differentiation against the stable HA scaffold [28].

4.4 Antibacterial Activity

Sr-HA produced modest but statistically significant antibacterial inhibition absent from the other three materials (4.3 mm vs S. aureus; 3.7 mm vs E. coli). The likely mechanisms involve localized pH elevation and competitive interference with bacterial Ca^{2+}-dependent metabolism. For more potent activity, co-doping with Zn^{2+} (0.6–1.0 mol%) alongside strontium provides substantial inhibition while preserving osteoblast cytocompatibility [14, 29], suggesting a clear direction for next-generation formulations.

4.5 Clinical Decision Framework

Based on the multi-parameter profile generated in this study, we propose the defect-matched clinical selection framework presented in Table 4.

4.6 Limitations

MG-63 cells do not fully replicate primary osteoblasts or hBMSCs; future work should include DPSCs and PDLSCs. Antibacterial testing used planktonic agar diffusion rather than biofilm models. Sr^{2+} release kinetics were not directly quantified by ICP-OES [30], nor was RT-PCR performed for osteogenic genes. Additional BCP ratios (20/80, 80/20) would map the full design space. No in vivo animal validation was performed; findings require confirmation in critical-size dental defect models before clinical recommendation.

Table 4. Proposed clinical decision framework for bioceramic bone substitute selection based on defect biology and regenerative objectives.

Clinical indication	Recommended material	Resorption priority	Rationale
ARP — healthy socket, intact buccal plate	β-TCP or β-TCP-rich BCP	Fast (4–6 months)	Complete substitution by host bone within implant placement window
Sinus floor elevation (delayed implant)	BCP 60/40	Moderate (6–9 months)	Best-evidenced balance of remodeling + volume stability; strongest RCT network meta-analysis support
Vertical/large augmentation, GBR	HA or BCP 80/20	Slow (>12 months)	Long-term scaffold integrity; low particle migration risk
Periodontal intrabony defects, peri-implantitis	Sr-HA (5 mol%)	Moderate	Combined osteopromotion, anti-resorptive, mild antibacterial; emerging translational data

ARP = alveolar ridge preservation; GBR = guided bone regeneration.

5 Conclusion

Under identical synthesis, sintering, and testing conditions, HA, β-TCP, 60/40 BCP, and 5 mol% Sr-HA exhibited distinct and complementary profiles. HA delivered the highest compressive strength (8.7 ± 0.6 MPa) and lowest degradation, best suited to long-term volume stability applications. β-TCP showed the fastest degradation and strong bioactivity but lowest mechanical strength. BCP offered a balanced profile supporting its dominant clinical role. 5 mol% Sr-HA provided the most favorable biological performance—highest MG-63 proliferation, ALP, mineralization, and the only antibacterial activity—while maintaining mechanical performance comparable to BCP. These findings support a defect-matched clinical decision framework and identify Sr-doped hydroxyapatite as the most promising next-generation bioceramic for combined osteopromotion, anti-resorptive, and antimicrobial applications. Confirmatory studies using primary stem cells, biofilm models, and preclinical animal models are warranted.

Conflict of Interest: The authors declare no conflict of interest.
Financing: The study was performed without external funding.
Ethical consideration: The study was approved by Babylon University, Hillah, Iraq.

REFERENCES

[1] Tan WL, Wong TL, Wong MC, Lang NP. A systematic review of post-extractional alveolar hard and soft tissue dimensional changes in humans. *Clin Oral Implants Res*. 2012;23(s5):1-21. doi: 10.1111/j.600-0501.2011.02375.x.

[2] Adams RJ. Is there clinical evidence to support alveolar ridge preservation over extraction alone? A review of recent literature and case reports of late graft failure. *Br Dent J*. 2022;233(6):469-74. doi: 10.1038/s41415-022-4967-2.

[3] Markets and Markets. Dental Bone Graft Substitute Market. 2026. https://www.marketsandmarkets.com/PressReleases/dental-bone-graft-substitutes.asp.

[4] Dorozhkin SV. Bioceramics of calcium orthophosphates. *Biomaterials*. 2010;31(7):1465-85. doi: 10.1016/j.biomaterials.2009.11.050.

[5] Stevens MM. Biomaterials for bone tissue engineering. *Mater Today*. 2008;11(5):18-25. doi: 10.1016/S369-7021(08)70086-5.

[6] Fendi F, Abdullah B, Suryani S, Usman AN, Tahir D. Development and application of hydroxyapatite-based scaffolds for bone tissue regeneration: A systematic literature review. *Bone*. 2024;183:117075. doi: 10.1016/j.bone.2024.

[7] Boskey AL. Bone composition: relationship to bone fragility and antiosteoporotic drug effects. *BoneKEy Rep*. 2013;2:447. doi: https://doi.org/10.1038/bonekey.2013.181.

[8] Horowitz RA, Mazor Z, Foitzik C, Prasad H, Rohrer M, Palti A. Î²-tricalcium phosphate as bone substitute material: properties and clinical applications. *J Osseointegration*. 2010;2(2):61-8. doi: 10.23805/jo.2010.02.02.04.

[9] Somngam C, Samartkit S, Kanchanasurakit S, Strietzel FP, Khongkhunthian P. New bone formation of biphasic calcium phosphate bone substitute material: a systematic review and network meta-analysis of randomized controlled trials (RCTs). *Int J Implant Dent*. 2025;11:47. doi: 10.1186/s40729-025-00636-4.

[10] Liu X, Huang H, Zhang J, Sun T, Zhang W, Li Z. Recent advance of strontium functionalized in biomaterials for bone regeneration. *Bioengineering*. 2023;10(4):414. doi: 10.3390/bioengineering10040414.

[11] Landi E, Tampieri A, Celotti G, Sprio S, Sandri M, Logroscino G. Sr-substituted hydroxyapatites for osteoporotic bone replacement. *Acta Biomater*. 2007;3(6):961-9. doi: 10.1016/j.actbio.2007.05.006.

[12] Tsai S-W, Hsu Y-W, Pan W-L, Hsu F-Y. The effect of strontium-substituted hydroxyapatite nanofibrous matrix on osteoblast proliferation and differentiation. *Membranes*. 2021;11(8):624. doi: 10.3390/membranes11080624.

[13] Cheng D, Ding R, Jin X, Lu Y, Bao W, Zhao Y, et al. Strontium ion-functionalized nano-hydroxyapatite/chitosan composite microspheres promote osteogenesis and angiogenesis for bone regeneration. *ACS Appl Mater Interfaces*. 2023;15(16):19951-65. doi: 10.1021/acsami.3c00655.

[14] Badea MA, Balas M, Popa M, Borcan T, Bunea A-C, Predoi D, et al. Biological response of human gingival fibroblasts to zinc-doped hydroxyapatite designed for dental applications—an in vitro study. *Materials*. 2023;16(11):4145. doi: 10.3390/ma16114145.

[15] Balamurugan A, Rebelo A, Lemos A, Rocha J, Ventura J, Ferreira J. Suitability evaluation of sol–gel derived Si-substituted hydroxyapatite for dental and maxillofacial applications through in vitro osteoblasts response. *Dent Mater*. 2008;24(10):1374-80. doi: 10.016/j.dental.2008.02.017.

[16] Bandyopadhyay A, Bernard S, Xue W, Bose S. Calcium phosphate-based resorbable ceramics: influence of MgO, ZnO, and SiO2 dopants. *J Am Ceram Soc*. 2006;89(9):2675-88. doi: 10.1111/j.1551-2916.2006.01207.x.

[17] Frasnelli M, Sglavo VM. Effect of Mg2+ doping on beta–alpha phase transition in tricalcium phosphate (TCP) bioceramics. *Acta Biomater*. 2016;33:283-9. doi: 10.1016/j.actbio.2016.01.015.

[18] Kokubo T, Takadama H. How useful is SBF in predicting in vivo bone bioactivity? *Biomaterials*. 2006;27(15):2907-15. doi:

10.1016/j.biomaterials.2006.01.017.

[19] Kokubo T, Yamaguchi S. Simulated body fluid and the novel bioactive materials derived from it. *J Biomed Mater Res A*. 2019;107(5):968-77. doi: 10.1002/jbm.a.36620.

[20] Champion E. Sintering of calcium phosphate bioceramics. *Acta Biomater*. 2013;9(4):5855-75. doi: 10.1016/j.actbio.2012.11.029.

[21] Frasnelli M, Cristofaro F, Sglavo VM, Dirè S, Callone E, Ceccato R, et al. Synthesis and characterization of strontium-substituted hydroxyapatite nanoparticles for bone regeneration. *Mater Sci Eng C*. 2017;71:653-62. doi: 10.1016/j.msec.2016.10.047.

[22] Capuccini C, Torricelli P, Sima F, Boanini E, Ristoscu C, Bracci B, et al. Strontium-substituted hydroxyapatite coatings synthesized by pulsed-laser deposition: in vitro osteoblast and osteoclast response. *Acta Biomater*. 2008;4(6):1885-93. doi: 10.016/j.actbio.2008.05.005.

[23] Bohner M, Santoni BLG, Döbelin N. β-tricalcium phosphate for bone substitution: Synthesis and properties. *Acta Biomater*. 2020;113:23-41. doi: 10.1016/j.actbio.2020.06.022.

[24] Liang H, Wang Y, Chen S, Liu Y, Liu Z, Bai J. Nano-hydroxyapatite bone scaffolds with different porous structures processed by digital light processing 3D printing. *Int J Bioprint*. 2022;8(1):502. doi: 10.18063/ijb.v8i1.502.

[25] Diez-Escudero A, Espanol M, Beats S, Ginebra M-P. In vitro degradation of calcium phosphates: Effect of multiscale porosity, textural properties and composition. *Acta Biomater*. 2017;60:81-92. doi: 10.1016/j.actbio.2017.07.033.

[26] Garrido CA, Lobo SE, Turíbio FM, LeGeros RZ. Biphasic calcium phosphate bioceramics for orthopaedic reconstructions: clinical outcomes. *Int J Biomater*. 2011;2011:129727. doi: 10.1155/2011/.

[27] Ran L, Liu L, Gao J, Pan Y, Ramalingam M, Du X, et al. Strontium-doped hydroxyapatite and its role in osteogenesis and angiogenesis. *Int J Dev Biol*. 2023;67(4):137-46. doi: 10.1387/ijdb.230091lc.

[28] Yang L, Perez-Amodio S, Barrère-de Groot FYF, Everts V, van Blitterswijk CA, Habibovic P. The effects of inorganic additives to calcium phosphate on in vitro behavior of osteoblasts and osteoclasts. *Biomaterials*. 2010;31(11):2976-89. doi: 10.1016/j.biomaterials.2010.01.002.

[29] Predoi D, Iconaru SL, Deniaud A, Chevallet M, Michaud-Soret I, Buton N, et al. Textural, structural and biological evaluation of hydroxyapatite doped with zinc at low concentrations. *Materials*. 2017;10(3):229. doi: 10.3390/ma10030229.

[30] Mocanu A, Cadar O, Frangopol PT, Petean I, Tomoaia G, Paltinean G-A, et al. Ion release from hydroxyapatite and substituted hydroxyapatites in different immersion liquids: In vitro experiments and theoretical modelling study. *R Soc Open Sci*. 2021;8(1):201785. doi: 10.1098/rsos.

How to cite this article

Al-Rihaymee S.; Comparative In Vitro Evaluation of Hydroxyapatite, β-Tricalcium Phosphate, Biphasic Calcium Phosphate, and Strontium-Doped Hydroxyapatite as Bioceramic Bone Substitutes for Dental and Maxillofacial Bone Regeneration. Future Dental Research (FDR). 2026;4(1):10-15. doi: 10.57238/fdr.2026.152576.1002